remote sensing

MDPI

Article

Characterisation of Sand Accumulations in Wadi Fatmah and Wadi Ash Shumaysi, KSA, Using Multi-Source Remote Sensing Imagery

ElSayed Hermas [1,2,*], Omar Alharbi [1], Abdullah Alqurashi [1], Abdoul Jelil Niang [1], Khalid Al-Ghamdi [1], Motirh Al-Mutiry [3] and Abudeif Farghaly [1,4]

[1] Geography Department, Umm Al-Qura University, Makkah 21955, Saudi Arabia; oaoharbi@uqu.edu.sa (O.A.); afalqurashi@uqu.edu.sa (A.A.); anniang@uqu.edu.sa (A.J.N.); kaghamdi@uqu.edu.sa (K.A.-G.); amfarghaly@uqu.edu.sa (A.F.)

[2] Applications of Physical Geology Department, The National Authority for Remote Sensing and Space Sciences (NARSS), Cairo 1564, Egypt

[3] Faculty of Arts, Princess Nourah bint Abdulrahman University, Riyadh 84428, Saudi Arabia; mkalmutairy@pnu.edu.sa

[4] Geology Department, Faculty of Science, Sohag University, Sohag 82524, Egypt

* Correspondence: eaibrahim@uqu.edu.sa; Tel.: +966-12-5494-5454

Received: 26 September 2019; Accepted: 25 November 2019; Published: 28 November 2019

check for updates

Abstract: The study area has three sand accumulations: Two in Wadi Fatmah and one in Wadi Ash Shumaysi, midwest of Saudi Arabia. The spatial extents of these sand accumulations have significantly increased over the last few decades. Multi-source satellite imagery, such as CORONA (1967, 1972), SPOT 5 (2013), LandSat TM (1986), and LandSat 8 OLI (2013), enabled monitoring and analysis of the interplay between the changes in the anthropogenic activities and spatial expansion of the areas of sand accumulation. The main driving force of the spatial expansion could be strongly linked to extensive changes in the anthropogenic regimes in the middle zone of Wadi Fatmah and its surrounding landforms and mountain masses. In this context, the once dominant agricultural lands of the middle zone of Wadi Fatmah have been transformed into abandoned agricultural areas. Extensive off-road driving has resulted in soil degradation. Excavation and mining activities for urban spatial expansion are widespread over the valley floor, the adjacent bajada, and the mountain blocks. These anthropogenic activities have remarkably induced strong wind erosion of the soil in severe arid conditions in the middle zone of Wadi Fatmah and Wadi Ash Shumaysi. Wind erosion has eventually produced a sufficient sand budget to be transported into the areas of sand accumulation. The primary consequence of the excess sand budget has been an increase in the spatial extents and dune migration rates of sand accumulations in the study area. However, this increase varies from one sand accumulation to another. In this study, we used multi-source remote sensing imagery and the state-of-the-art COSI-Corr technology to characterize sand accumulations in the study area and to determine the spatio-temporal changes in both the spatial extents and the dune migration rates. The mean annual migration rates of sand dunes in the three sand accumulations ranged from 5.5 and 7.2 to 8.6 m/yr. Analysis of the spatial extent and migration rates of sand accumulations indicates that the study area may have experienced desertification in response to changes in the anthropogenic regimes through the last few decades.

Keywords: dune migration; COSI-Corr; hazards; remote sensing; Makkah; Saudi Arabia; ASTER

1. Introduction

In response to sparse vegetation cover and the availability of sand supply, wind acts in arid regions to form sand accumulations [1]. They can develop in a variety of local environments, such as coastal areas [2], low-land depressions [3,4], and over valley floors in a mountainous landscape [5]. Dune fields in mountainous landscapes normally exist in association with major wide valleys and move against or into the foothills of mountain escarpments [5,6]. Topography, landforms, and the vegetation cover of the mountain landscape, along with human activities, can all play a critical role in controlling wind and sand supply characteristics.

Topographic characteristics, such as the relative elevations and slope magnitude and aspect, can greatly affect the intensity and direction of local wind [7,8], rather than their roles as potential obstacles in front of winds, allowing sand deposition [9,10]. Alluvial landforms, such as the alluvial plains, bajada, and the weathered sedimentary formation of the mountain masses, can represent potential sources of sand supply to sand accumulation in mountain landscapes [1,11–15].

In addition to the impact of topography and landforms on the formation and development of sand accumulations, both natural and agricultural vegetation significantly influence sand supply and dune mobility. Vegetation can play a dual role in the aeolian processes—its absence may increase soil erosion and dune mobility while its presence can minimize soil erosion and accordingly the magnitude of sand mobility [16–19]. There are many factors that control the role vegetation will contribute in aeolian processes. Anthropogenic activities are considered a potential factor that could result in significant disturbances to the plant community and soil in a given geographic area [20,21]. Anthropogenic activities can drastically deteriorate both natural and agricultural vegetation, resulting in severe soil erosion by winds [22–26]. These anthropogenic disturbances might extend to off-road driving and overgrazing [27], and excavation and mining activities [28,29]. Both activities have been recorded and documented in many areas across the world as direct driving forces of land degradation. These activities significantly contribute to the sand budget of a given sand accumulation. In this context, the study area has experienced a severe retreat in natural and agricultural vegetation over the last few decades in response to various and extensive unmanaged anthropogenic activities. Multi-source remote sensing imagery and advanced digital image-processing techniques can help monitor and map the morphologic and anthropogenic characteristics of a given geographic area and their influences on the spatio-temporal changes of sand accumulations.

Earth observation satellites have served the community by providing a systematic and long archive of remote sensing images over the last 50 years. They have enabled scientists to carry out many dune-related studies, such as dune mapping and taxonomy [30,31], pattern analysis of dune fields [32–34], spatial analysis of dune fields [35,36], topographic and morphologic variations of dune fields [37–39], mineralogic and sedimentologic characteristics [40], and climatic changes [41]. In addition to these studies, the determination of the rates of dune migration has received particular emphasis from remote sensing application scientists in the field of geomorphology (e.g., [42–52]). From this perspective, two or more remote sensing images are accurately georeferenced and then dune boundaries or axes are delineated for eventual comparison of the boundaries and axes to calculate the lateral displacement of sand dunes. In contrast to in-situ field measurements, the determination of dune migration rates using georeferenced remote sensing images allows the dune migration to be constrained over a wide spatial coverage. However, this classical approach to defining dune boundaries using remote sensing images is highly affected by satellite geometry and illumination conditions [53], along with the effect of personal bias through the definition and delineation of dune boundaries [36].

Recent advances in remote sensing techniques have submitted the co-registration of optically sensed images and correlation (COSI-Corr) as an alternative pixel-wise quantitative approach to dune migration. This approach relies on correlating two or more ortho-rectified images using spatial cross-correlation to produce displacement images where the values and signs of each pixel express the amount of surface displacement (in meters) and its direction, respectively. The approach was submitted to the scientific community by Leprince et al. [54]. Recently, it has been used in many studies for the purpose of determining dune migration rates and directions [55–60].

In this research, we aimed mainly to characterize the climatic, morphologic, and anthropogenic parameters that contribute to the changes in the spatial extents and dune migration rates of sand accumulations in the study area using multi-source remote sensing images and the COSI-Corr technology. The results of this study will provide an outline of the temporal and spatial characteristics of the aeolian activity in the study area, which can help local authorities and environmental planners avoid its consequences in the future.

2. Study Area

Makkah City and its surroundings mainly comprise granitic basement rocks that belong to the Precambrian. In the north and east of Makkah City, sedimentary rocks are represented as well. Complex sets of faults and fractures characterize the area and imply a long tectonic history. These sets occur either parallel or perpendicular to the direction of the Red Sea. Since the initiation of the tectonic processes in the Tertiary Period, both basement and sedimentary rocks have been uplifted, resulting in rugged topographic mountains that range in elevations from 200 to 400 m asl. Well-developed surface stream networks have incised the rugged mountains, developing many drainage basins around Makkah City. The largest is Wadi Fatmah, which bounds the city from the north and west. The study area is located in the main transportation system of Wadi Fatmah drainage basin and along Wadi Ash Shumaysi, which is a wide structural depression perpendicular to the transportation system of the Wadi Fatmah drainage basin (Figure 1). Sand accumulations occupy significant patches at the southern edges of the Wadi Fatmah trunk valley, and along Wadi Ash Shumaysi (Figure 1). The spatial extents of these sand accumulations have recently experienced significant spatial changes. These changes could be linked strongly to various human activities that have taken place over the last few decades.

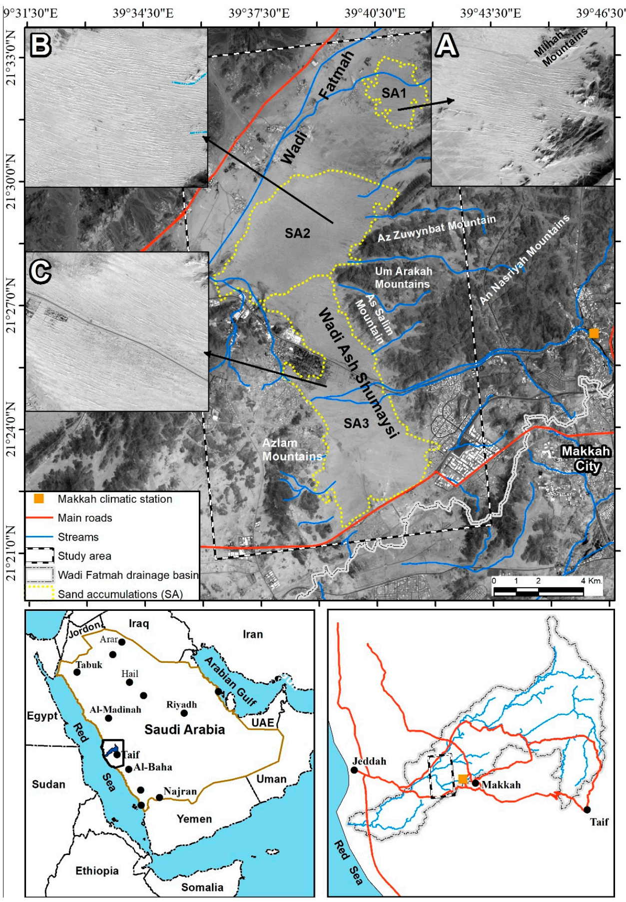

Figure 1. Location of the study area in Saudi Arabia; A, B, and C are selected samples of sand accumulations (SA1, SA2, SA3).

3. Data and Method

3.1. Data Acquisition and Preparation

We used different multi-source remotely sensed data in this research—namely, CORONA, SPOT 5, ASTER, Landsat images, and digital elevation model (DEM). The intelligence project CORONA, which was declassified in 1990 [61], provides a potential historical source for long-term earth observation. For this research, CORONA images taken in 1967 and 1972 were acquired over the study area. As a panchromatic image, automatic extraction of the land features cannot be done using such data [62]; thus, CORONA images were only used to visually delineate the spatial characteristics of the various spatial features, such as morphological and human features in the past. We used a SPOT 5 image acquired in 2013 from the King Abdulaziz City for Science and Technology (KACST) to monitor the changes of the spatial distribution and extent of sand accumulations over the last decades in the study area. The Landsat Thematic Mapper (TM) of 1986 and the Landsat Operational Imager (OLI) of 2013, acquired from the United States Geological Survey (USGS) Global Visualization (GloVis) site, were used for visual interpretation. Heads-up digitizing of the various morphological features, such as sand accumulations, landforms, and human-made features, was carried out using both CORONA and SPOT 5 images. Topographic analysis of the study area was conducted as well, using 1 arc sec digital Elevation model (DEM) acquired by the Shuttle Radar Topography Mission (SRTM). The migration rates of sand dunes of the various sand accumulations in the study area were determined using five ASTER images of a spatial resolution of 15 m that were collected from the United States Geological Survey (USGS) Global Visualization (GloVis) site. These images were acquired in November 2011, 2012, and 2013, and September 2014 and 2015. Table 1 presents the technical specifications of the acquired ASTER images. They have almost similar pointing and orientation angles, which is suitable for achieving successful correlation results. Finally, we obtained meteorological data on the study area between 1985 and 2014 from the General Authority of Meteorology and Environmental Protection, KSA.

Table 1. Technical specifications of Advanced Spaceborne Thermal Emission and Reflection Radiometer (ASTER) images used in the study.

Acquisition Dates	Pointing Angle	Orientation Angle	Sun Azimuth Angle	Sun elevation Angle	Spatial Resolution
November 09, 2011	−8.58	8.80	155.79	48.64	15
November 27, 2012	−8.59	8.80	157.48	43.94	15
November 14, 2013	−8.59	8.80	156.87	47.20	15
September 30, 2014	−8.58	8.80	142.38	60.15	15
September 24, 2015	2.87	8.80	141.049	62.855	15

3.2. Determination of Dune Migration

All ASTER images were accurately ortho-rectified for eventual sub-pixel spatial cross-correlation using the typical processing chain of COSI-Corr technology. The COSI-Corr is a plug-in ENVI® digital image processing software. The ortho-rectification process involved careful selection iteratively of the tie points between a previously ortho-rectified image and a slave image (the raw image) [63]. The tie points were then converted into ground control points (GCPs) and eventually optimized using the reference image, a free sinks Shuttle Radar Topographic Mission digital elevation model (DEM), and the ancillary file of each image containing the various parameters of ASTER LA1 sensor system to produce five ortho-rectified images (Figure 2). After the ortho-rectification processes, the COSI-Corr correlation engine was then automated to correlate the ortho-rectified images consecutively. In this way, we arrived at four correlation pairs: 2011–2012, 2012–2013, 2013–2014, and 2014–2015. For each pair, we adopted the same correlation parameters, which were multi-scale window sizes ranging from 64 to 32 pixels, and a 2-pixel shifting step between the sliding windows. The correlation of each pair produced a horizontal displacement image comprising three bands: East-west displacement band, north-south displacement band, and signal-to-noise ratio band. To remove the noise values from the displacement bands and the signal-to-noise ratio band, we applied the non-local means filter [64]. The pixels of the east-west (E-W) and the north-south (N-S) displacement bands comprised values and signals. The values refer to the pixel displacement between the master and slave images of each correlation pair, while the signals denote the direction of such displacement. For instance, the positive values indicate the amount of pixel displacements in the east and north whereas the negative values indicate the amount of pixel displacements in the west and south. The east-west and north-south displacement bands were integrated to calculate the net annual migration rates, using the approach proposed by Necsoiu, Leprince, Hooper, Dinwiddie, McGinnis, and Walter [57]. In addition, we carried out two days of fieldwork to explore the data extracted from visual interpretation and to collect signals of land degradation, such as soil cracks. Figure 3 presents a flowchart demonstrating the whole approach adopted to achieve the aims of this research.

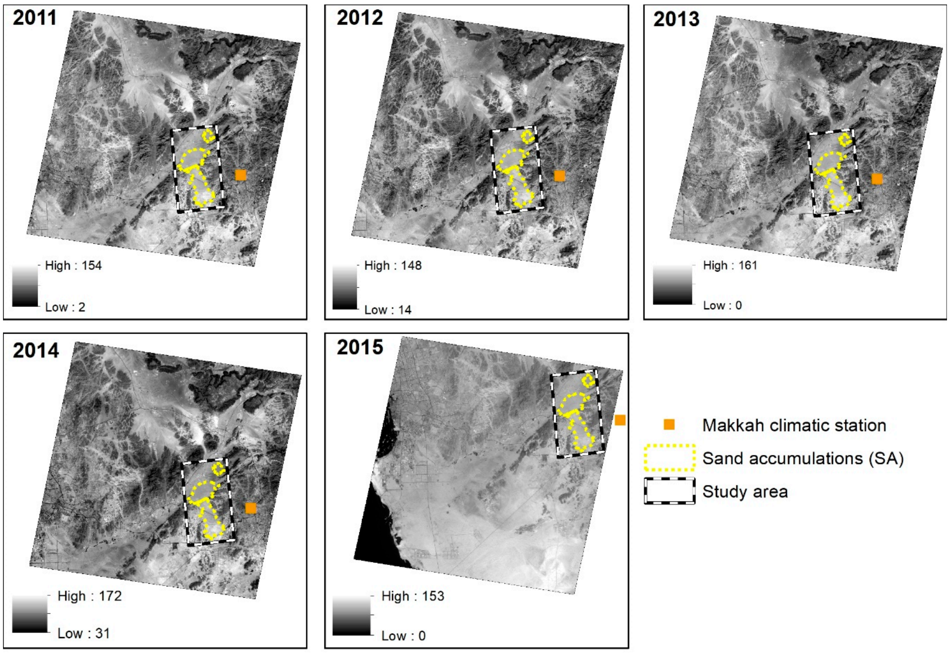

Figure 2. Five ortho-rectified and co-registered ASTER images.

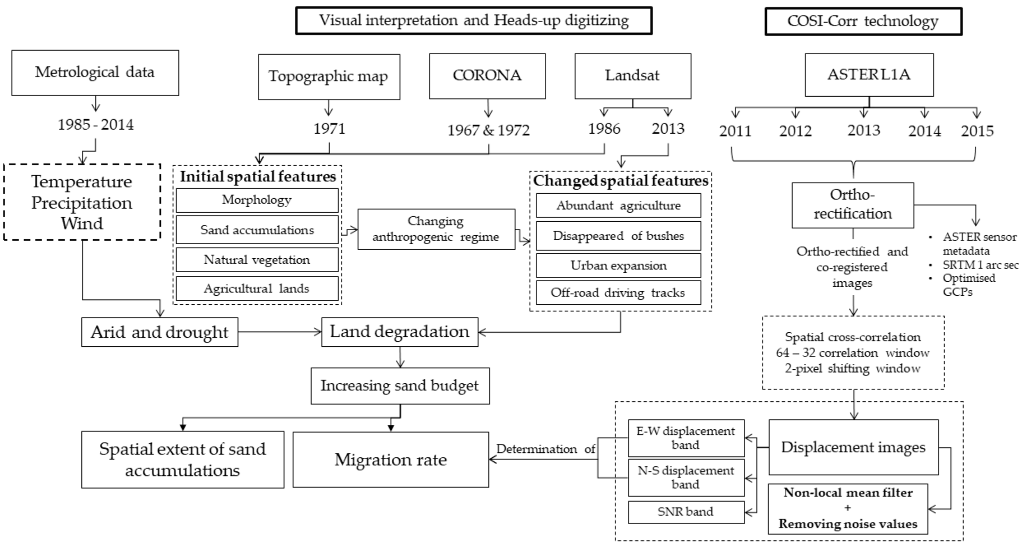

Figure 3. A flowchart of the adopted approach in this research.

4. Results

4.1. Climatic Parameters of the Study Area

The study area is characterized by a typical desert environment where the temperature is high and rainfall is low [65]. The climatic investigation carried out on the study area indicated the dominance of arid conditions. The mean annual temperature rates ranged from 24.8 to 38.2 °C. Summer is characterized by the highest seasonal values of temperatures (Figure 4). The mean of the minimum temperature of summer was 29.2 °C, whereas the mean of the maximum temperature of summer was high, reaching 43.2 °C. On the other hand, the mean seasonal rates of the temperature in winter ranged from 19.5 to 31.5 °C. Al-Harbi [66] used the temperature data collected from all climatic stations located within and around the Wadi Fatmah drainage basin to produce a distribution map of the temperature. The map demonstrated that the highest temperature values were limited to the middle zone of the Wadi Fatmah basin, which is where our study area is located.

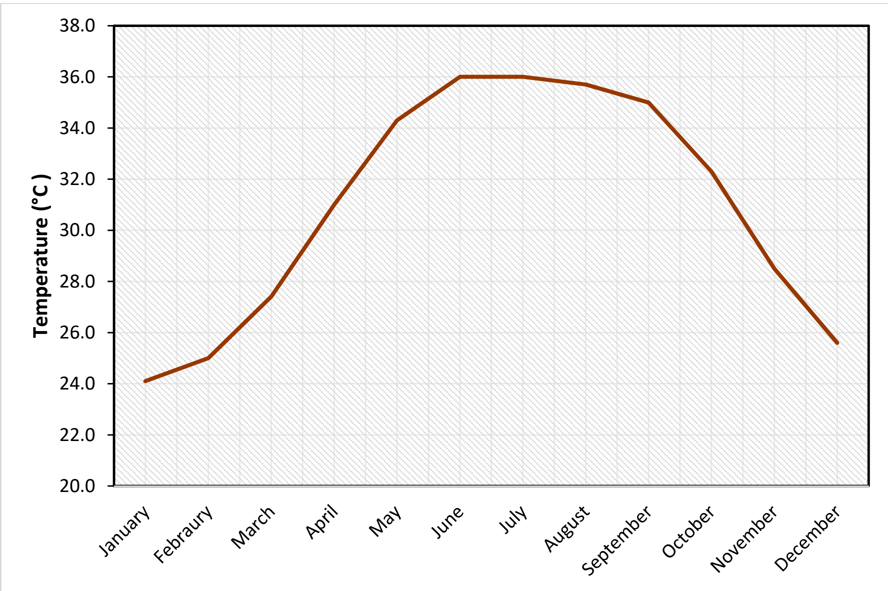

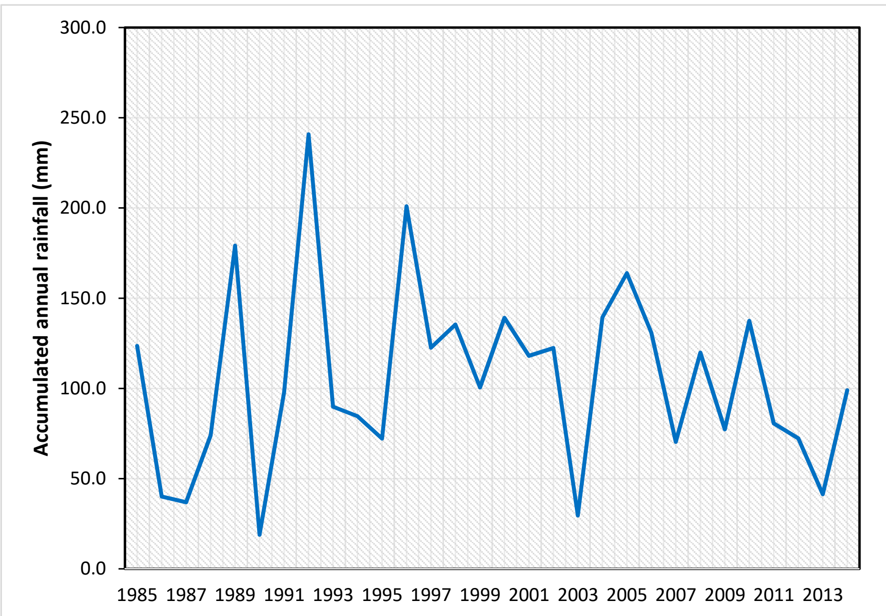

Figure 4. The monthly mean of temperature (up) and the accumulated annual amounts of rainfall (down).

Rainfall is another factor that controls arid conditions in a given geographic area. Spatially, the amount of rainfall significantly varies in the Wadi Fatmah drainage basin. It increases in the upstream reaches where elevations are high, and decreases downstream [67]. The rainfall in the upstream reaches exceeds the arid rainfall threshold, reaching ~279 mm/year [67]. On the other hand, the middle area of Wadi Fatmah basin where the study area is located is characterized by limited rainfall amounts ranging from 80 to 100 mm/year [66–68] (Figure 4). The limited amounts of rainfall associated with high temperature values outweigh the opportunity for arid conditions to dominate in the study area. This setting could potentially be affirmed by the recorded high evaporation rates. The recorded annual rate of evaporation was 3560 mm/year [66], which exceeds many times the precipitation rate in the study area, denoting strong arid conditions. These conditions could potentially result in a significant water deficit [69]. In this context, wind action transports sand fragments to the study area and deposits them there. Exploration of wind data records indicated that the study area experiences an unidirectional wind regime from the north direction (Figure 5). The northern wind strongly increases in summer, winter, and spring in the order of ~83%, 62%, and 59%. In autumn, the northern wind decreases to 32% in favor of the southern and southwestern winds, which record 45% and 23% of the total wind, respectively [66]. In addition to the arid conditions that trigger strong aeolian processes, geomorphic features have also helped initiate and develop sand accumulations in the study area.

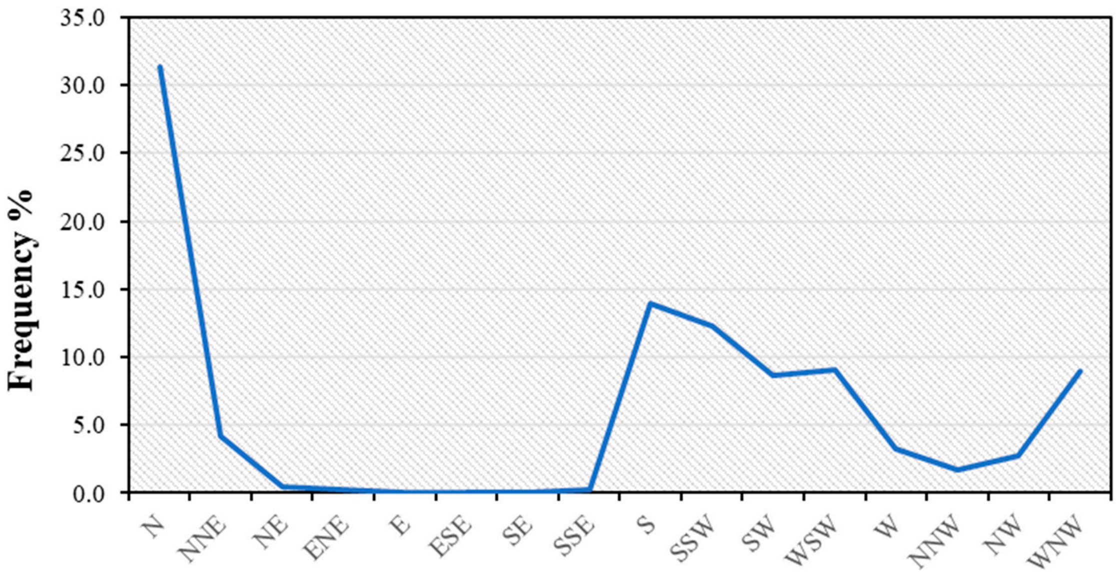

Figure 5. The frequency of winds through the various wind directions.

4.2. Morphology of the Study Area

The study area comprises various geomorphic landforms, including mountain ridges, folded mountains masses, isolated hills, bajada, and alluvial plains (Figure 6). The mountain ridges are located in the east, southeast, and southwest of the study area. Lithologically, the mountain ridges mainly comprise hard basement rocks of granitic composition along with metamorphic rocks, such as schists and gneisses. The majority of the mountain ridges are structurally controlled, and aligned either in the NE-SW, N-S, or E-W directions (Figure 6). The ridges are considerably eroded to various extents, and mainly separated from each other by intermittent streams (Figure 6). The SW mountain ridges are separated from the SE mountain ridges by a structurally controlled wide depression, which is known locally as Wadi Ash Shumaysi (Figure 6). The depression trends in the NW-SE direction and is filled with alluvial deposits transported from the adjacent eastern and western mountain blocks by infrequent surface runoff. To the north and almost perpendicular to the trend of Wadi Ash Shumaysi lies the alluvial plain of Wadi Fatmah. It trends in the NE-SW direction (Figure 6). North to the alluvial plain of Wadi Fatmah, three salient mountain masses occur, which are Jabal Sidr, Jabal Mikassar, and Jabal Daf

(Figure 6). These folded mountain masses consist of un-metamorphosed to low-grade metamorphosed sedimentary rocks known as the Fatmah Group [70]. At the foot-slope of each mountain mass, bajada surfaces have been developed as prominent morphologic features in the study area (Figure 6). The bajada surfaces occupy a considerable spatial extent in the order of ~24 km^2. Although the bajadas occupy extensive areas in front of the three northern mountain masses, they are produced from small catchments (Figure 6). The production of these considerable bajada surfaces from small catchments clearly implies that the three mountain masses are highly erodible surfaces, which could represent potential source areas for detrital sand to be transported by the dominant northern wind in the study area. This hypothesis could be supported not only by the lithologic composition of these mountains but also by the topographic characteristics of the study area.

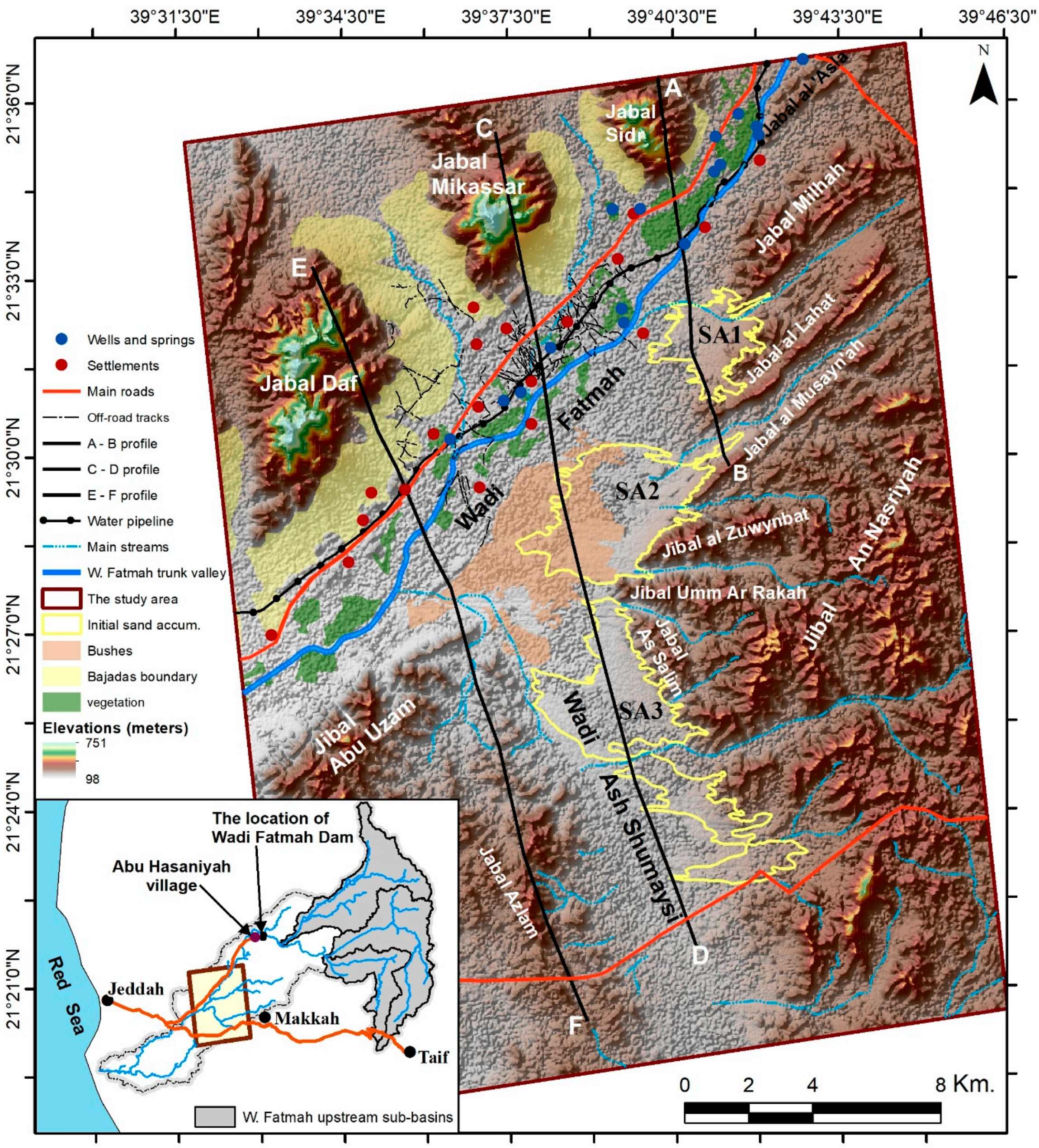

Figure 6. The major morphologic features in the study area demonstrated on a 30 m Digital Elevation Model (DEM); A-B, C-D, and E-F are the spatial locations of the transects of topographic profiles shown in Figure 7.

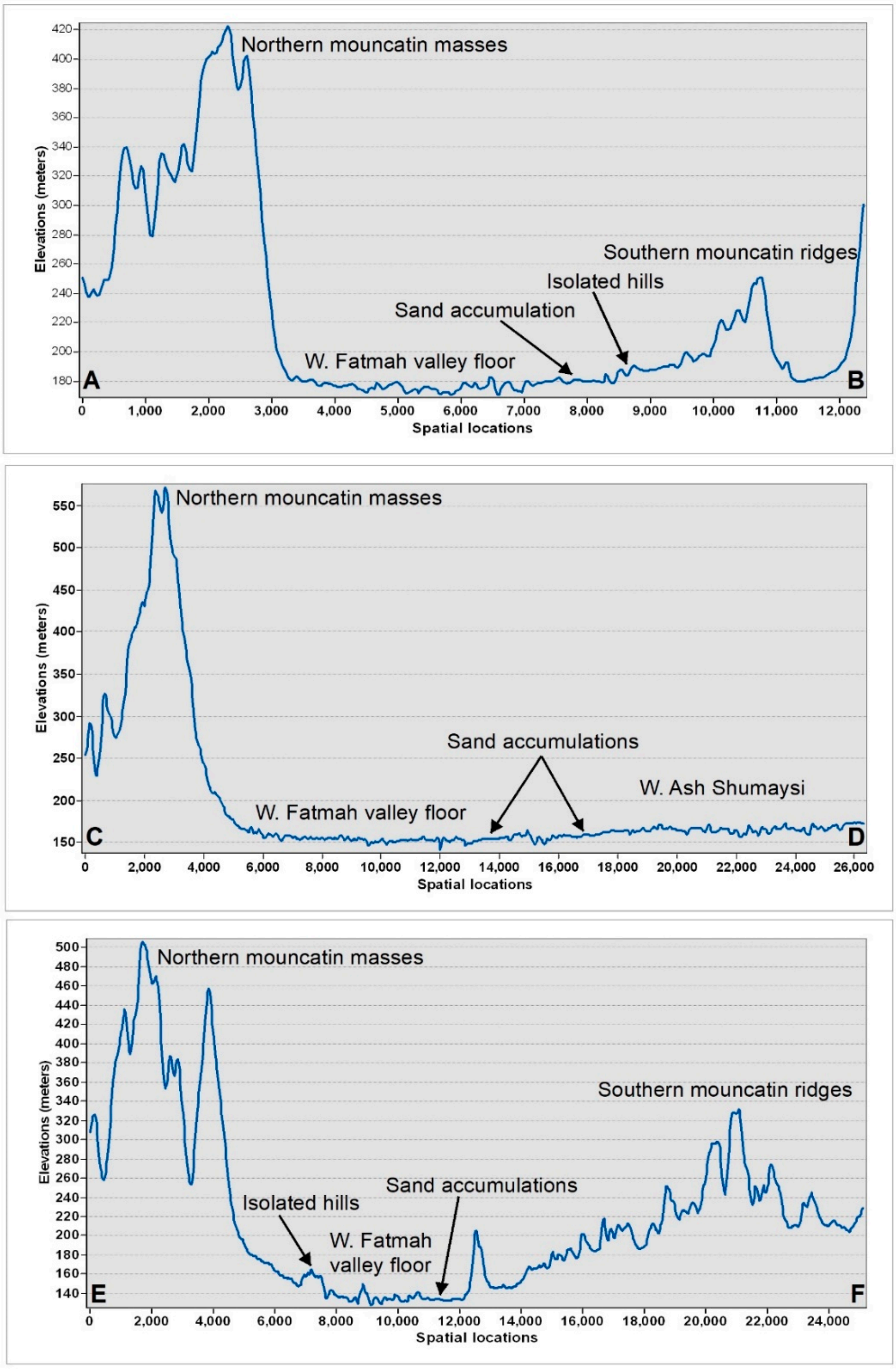

Figure 7. The topographic profiles in the study area; A-B, C-D, and E-F represents of the spatial locations of the topographic transects shown in Figure 6.

Three N-S topographic transects were extracted from the digital elevation model of the study area (Figure 7). All topographic transects disclose significant variations in the elevation where the northern mountain masses are notably higher than the southern mountain ridges in the study area. The elevation differences, along with the high erodibility of the northern mountain masses, qualify these masses to be potential sources of detrital sand to be transported southward. While the northern mountain masses function as source areas of aeolian sands, the southern mountain ridges with their orientations could efficiently function as topographic obstacles for wind-transported sands (Figure 7). In addition, the satellite imagery, field observation, and topographic transects all assert to the presence of many other obstacles for wind-transported sand from the northern mountain masses. One of these potential obstacles is the isolated hills (Figure 8). The role of the isolated hills as obstacles that could initiate and help in the development of various dune forms is well monitored and documented [10,71]. In front of all mountain ridges that flank the southern edges of the alluvial plain of Wadi Fatmah, more than 100 NE-SW-trending isolated hills exist (Figure 8). Climbing dunes and leeward-extended dunes occur windward and leeward of the isolated hills, respectively. The topographic transects denote that the alluvial plains of Wadi Fatmah and Wadi Ash Shumaysi are undulated surfaces as well (Figure 7), which qualifies them as potential obstacles against wind-transported sands. Over these undulated surfaces, especially in low topography areas, wide areas of bushes (scrub) were monitored using the Corona satellite image acquired in 1972 (Figure 8).

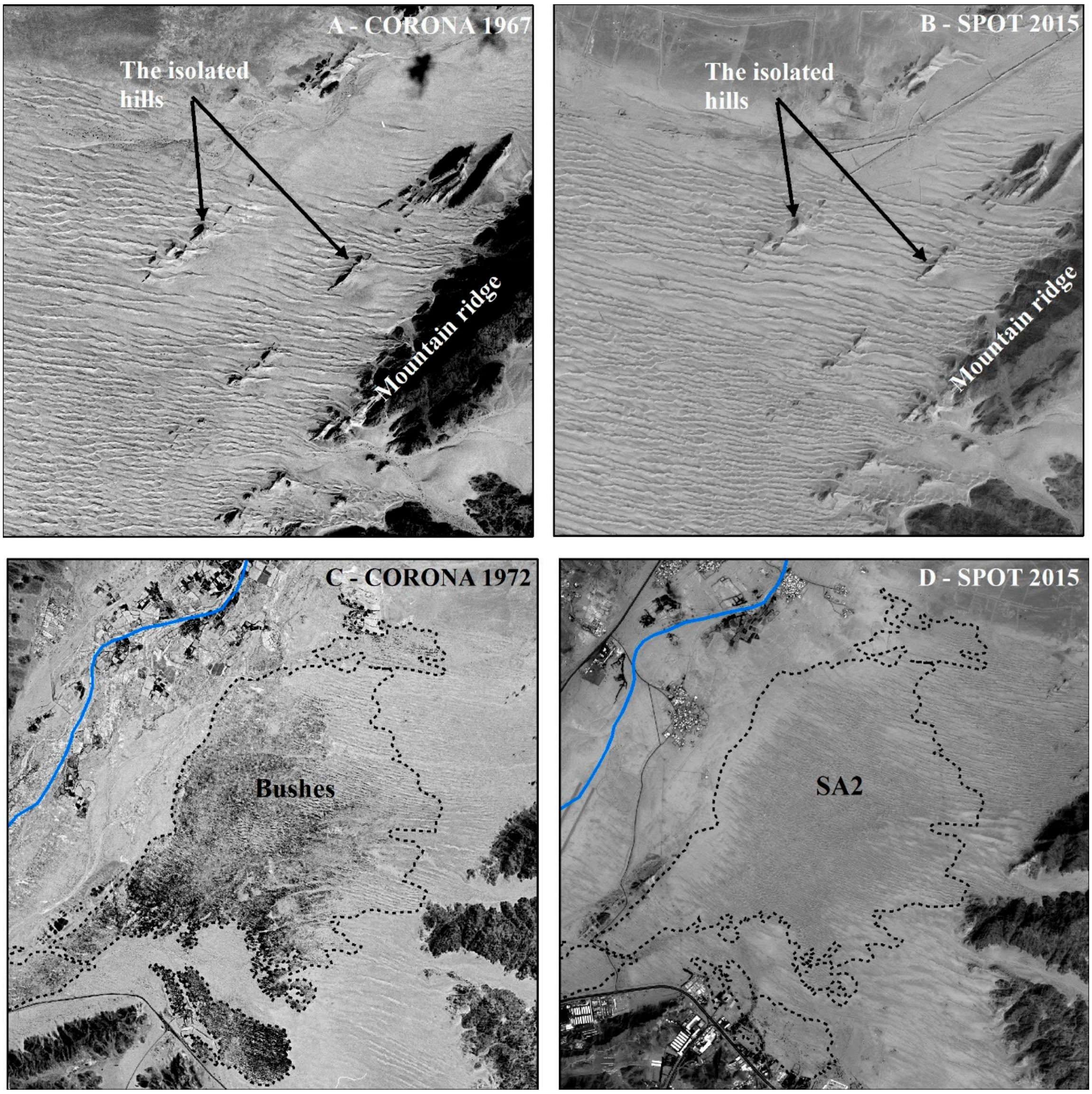

Figure 8. The impact of both isolated hills and mountain ridges on sand accumulations (as shown from the comparison between the upper left image A-Corona 1967 and the upper right image B-SPOT 5 2015) and the shrinking of both natural and agricultural vegetation in favor of the formation of sand accumulations (as shown from the comparison between the lower left image C-Corona 1972 and the lower right image D-SPOT 5 2015).

The total area of these bushes is ~19 km^2. The density of the bushes is spatially varied. It increases westward where the main trunk course of Wadi Fatmah exists, and significantly decreases eastward where dunes dominate (Figure 8). The topographic maps of 1971 also demonstrate significant agricultural areas in the order of 14 km^2 occupying the middle zone of the Wadi Fatmah alluvial plain around the main course of the trunk valley (Figures 6 and 8). The extensive areas of both agricultural and natural vegetation clearly indicate that the alluvial plain was receiving an appropriate water supply that kept the soil moist enough for plants to grow. Maintaining soil moisture would reduce wind erosion, and accordingly minimize the production of wind-transported sands from the alluvial plain of Wadi Fatmah. Therefore, sand supply to the area of sand accumulations was mostly attributed to the elevated and highly erodible mountain masses in the north of the alluvial plain. Under such conditions, the initial sand accumulations developed in the study area (Figure 6).

The initial sand accumulations that were determined from the Corona images can be labelled SA1 (sand accumulation 1), SA2 (sand accumulation 2), and SA3 (sand accumulation 3) (Figure 6). The entire spatial extent of all the initial sand accumulations was in the order of 40 km^2. SA1 is the smallest and SA3 is the largest, extending over 18.7 km^2. Both SA1 and SA2 occupy low elevations and slopes in the southern flank of the alluvial plain of Wadi Fatmah. They extend against the NE-SW mountain ridges and the numerous isolated hills in front of these ridges (Figure 8). While SA1 and SA2 have developed in front of the mountain ridges in the east of the study area, SA3 has developed in the wide depression of Wadi Ash Shumaysi between the mountain blocks of the SE and SW reaches of the study area. In the depression, a low-energy wind is possibly stimulated, which allows aeolian processes to develop sand dunes on the floor of the depression. Although sand accumulations in the study area occupy different places, they extend in the southeast direction against hillslopes of the mountain ridges and the isolated hills, indicating the impact of the local topographic setting on the dominant northern wind regime. The above characteristics of the climatic and morphologic features have controlled the formation of the initial sand accumulations in the study area. Through the last few decades and in response to massive changes in the anthropogenic changes, these initial sand accumulations have extensively expanded, with significant high rates of dune migration.

5. Discussion

5.1. Anthropogenic Activities in the Study Area

A review of the previous literature, along with an analysis of the available satellite images, might help define the relationship between human activities and the increasing sand budget in the study area over the last few decades. The principal human activity in Wadi Fatmah drainage basin for a long time has been agriculture. Until 40 years ago, Wadi Fatmah valley was the main source of various agricultural crops for the major surrounding big cities, such as Makkah, Taif, and Jeddah [72]. In this context, the middle zone of Wadi Fatmah, in which the study area is located, was producing more than 40% of all the agricultural farms of Wadi Fatmah [73]. The primary source of water for the agricultural and other domestic activities in the middle zone of Wadi Fatmah was the underground water discharged from shallow alluvial aquifers [67,73]. Water discharge for agricultural activities and associated domestic practices primarily relied on water springs, which were well-known features in the Wadi Fatmah drainage basin. Over the last six decades, the number of these springs has decreased significantly from about 400 to only 5 [73]. The drastically decreasing number of water springs is mainly attributed to a massive unmanaged discharging strategy adopted in the 1970s to meet the domestic fresh-water requirements of Makkah and Jeddah cities. This strategy required the construction of new water wells to discharge fresh water from the alluvial aquifers through water pipelines to these cities [73]. The direct consequence of this water-discharging strategy was the decreasing water level of the alluvial aquifers, and accordingly, the shrinkage of the number of water springs. In addition, the alluvial aquifers have experienced a severe lack of replenishment over the last decades as a result of the construction of the Wadi Fatmah Dam in 1985 (Figure 6). The dam is located at Abu Hasaniyah village where surface runoff of three major upstream sub-basins accumulates (Figure 6). According to the Ministry of Water, Environment, and Agriculture, the dam is designed to store 20 million m^3 of fresh water annually. The surface runoff of these upstream sub-basins was the principal source of replenishment of the alluvial aquifers in the middle zone of Wadi Fatmah drainage basin, including the study area [73]. Under such conditions, water required for agricultural practices has undergone a drastic loss over the last few decades, eventually resulting in the transformation of ~19 km^2 of agricultural lands into abandoned agricultural areas (Figure 9), allowing the era of land degradation to start. Therefore, vegetation cover has diminished, and deficit soil moisture levels have been sustained [23,74–76]. The reduction in both vegetation cover and soil moisture content has resulted in intense wind erosion [22,23,25,26] that has made the sand grains easily detach and be transported by the wind [17]. Visual interpretation of the 1972, 1986, and 2013 images demonstrates a substantial reduction in both natural and agricultural vegetation cover (Figure 9). Observations from fieldwork reveal the presence of drought signals, such as soil cracks (Figure 9). These cracks are widely distributed in the area of bushes, implying a sustained deficit in soil moisture. These indices could potentially indicate that the study area might have experienced serious drought conditions through the last decades in response to the common arid conditions and the changes in the un-managed and planned anthropogenic changes. Accordingly, most natural vegetation cover has been extensively transformed into mobile sand dunes, while the majority of the agricultural lands have become bare land or been replaced by other anthropogenic activities (Figure 9).

In addition, many other anthropogenic activities can increase the rate and amount of sand supply in a given geographic region. These activities may include off-road driving [27], intense grazing [77], and excavation for construction purposes [28,29]. Figure 6 demonstrates the presence of a considerable number of off-roads on both the northern and southern alluvial plains around Wadi Fatmah trunk valley, along with the presence of recent off-roads over the surfaces of the alluvial fans in the northwest of the study area. A comparison of the satellite images discloses a tangible urban spatial expansion either on the valley floor, over the surface of the alluvial fans, or over the mountain masses in the northwest reaches of the Wadi As Shumayi depression (Figure 9). Urban spatial expansion over the mountain masses normally requires fragmentation and removal of detrital sediments before urban construction (Figure 9). This process of excavation could have released a significant amount of fine sands that may have participated in the expansion of sand accumulations [29] in the study area. The above characterization of the various climatic, morphologic, and anthropogenic activities in the study area shows intense soil erosion constraints that could result in a significant sand supply for aeolian saltation processes [23,24]. With the increase of the sand supply, the spatial extent of sand accumulations is highly expected [10], and sand dune development and migration rates can intensify as well [29,78]. Both the spatial extent and dune movement of the three sand accumulations in the study area were monitored using COSI-Corr technology.

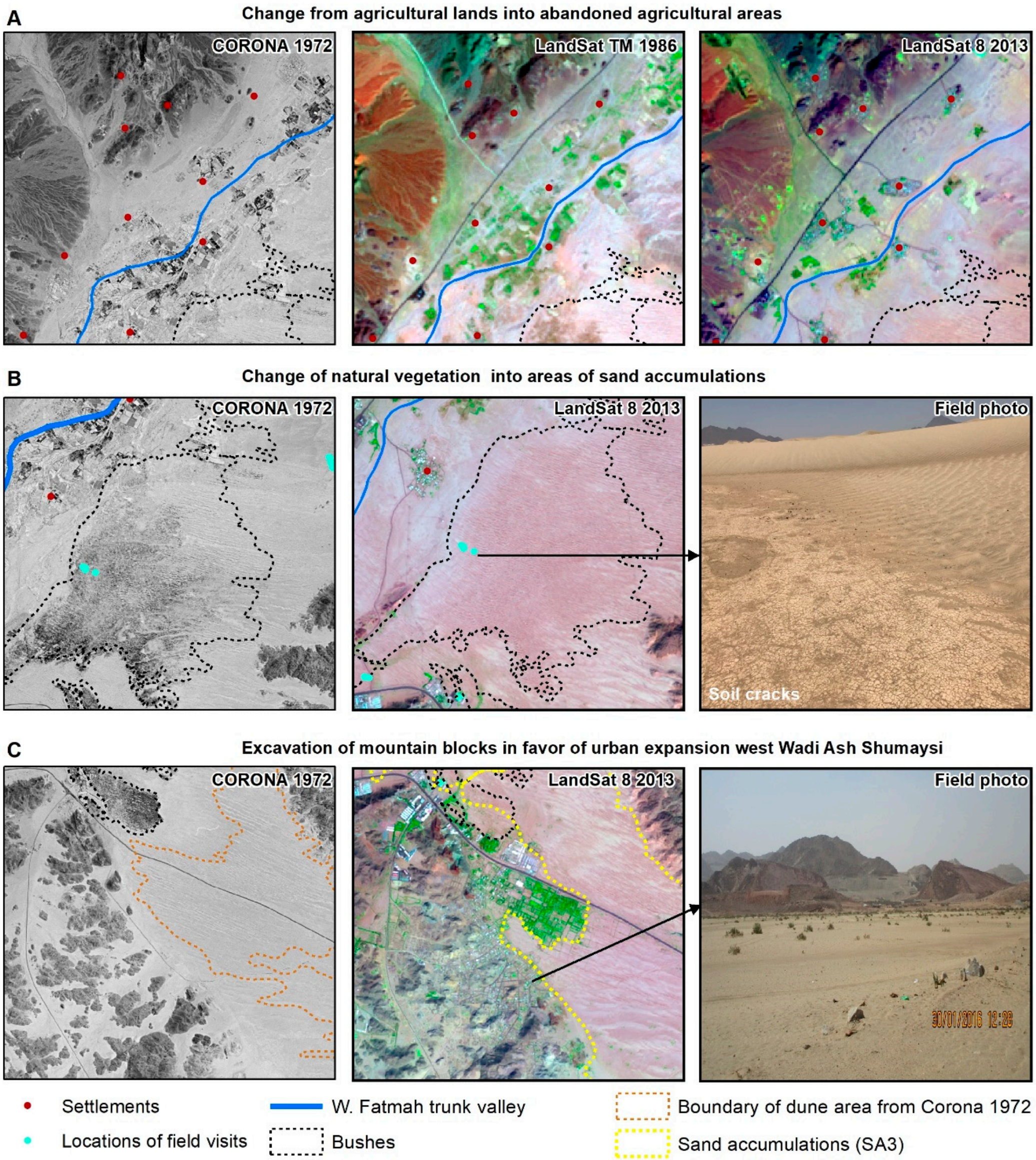

Figure 9. Multi-source satellite imagery at different dates show significant shrinkage of both agricultural and natural vegetation (row A and B) and spatial urban activities at the expense of the adjacent mountain block (row C).

5.2. Dune Migration Rates of Sand Accumulations in the Study Area

The correlation process between five ortho-rectified ASTER images produced four correlation images, which are the 2011–2012, 2012–2013, 2013–2014, and the 2014–2015 images (Figure 10). Each correlation image comprises E-W and N-S displacement bands (Figure 10) along with the signal-to-noise ratio (SNR) band. The pixel values of the E-W and N-S bands express pixel displacements between the input ortho-rectified ASTER images. Table 2 demonstrates the descriptive statistics of the pixel values of the E-W and N-S displacement bands. The mean values of pixel displacements of the E-W bands recorded higher values than the N-S displacement bands of all the correlation images (Table 2). In addition, the mean values of the E-W displacements bands are characterized by positive signs whereas the mean values of the N-S displacements values are characterized by negative signs. The mean values and signs of the E-W and N-S bands indicate that the overall pixel displacements tend to be in the southeast. To determine the net annual displacement in the study area, we integrated the E-W and N-S displacement bands of each correlation image using the approach proposed by Necsoiu et al. [79]. The integration produced four images representing the annual rates of pixel displacements in the study area from November 2011 to September 2015 (Figure 11). The figure indicates that the highest values of the annual rates of pixel displacement are associated with the three sand accumulations in the study area, indicating dune migration on an annual scale. The pixel displacements of the three sand accumulation areas were averaged to produce dune field statistics for the purpose of studying the spatial and temporal patterns of dune migration in the study area.

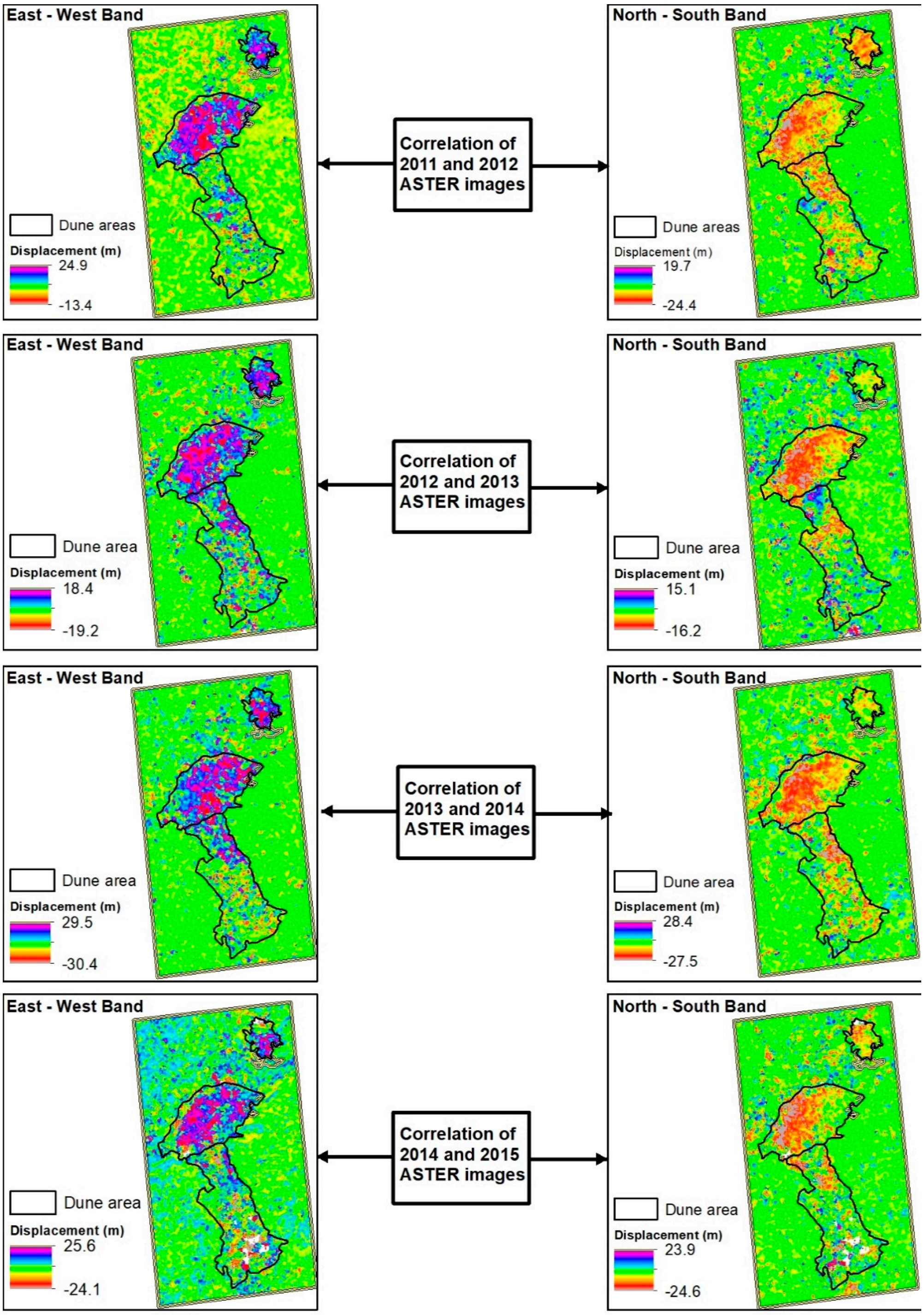

Figure 10. The E-W and N-S bands produced from the correlation of the ortho-rectified and co-registered ASTER images.

Table 2. Statistics of the values of pixel displacements of the produced E-W and N-S displacement bands of the correlation pairs.

Statistics	Correlation Pairs							
	2011–2012		2012–2013		2013–2014		2014–2015	
	E-W	N-S	E-W	N-S	E-W	N-S	E-W	N-S
Min.	−13.47	−24.48	−19.22	−16.27	−30.44	−27.5	−24.16	−24.61
Max.	24.94	19.75	18.48	15.18	29.54	28.46	25.61	23.95
Mean	1.22	−0.38	0.76	−0.38	0.79	−1.03	1.82	−0.83
SD	4.22	2.52	2.97	2.29	3.63	2.91	3.79	3.01

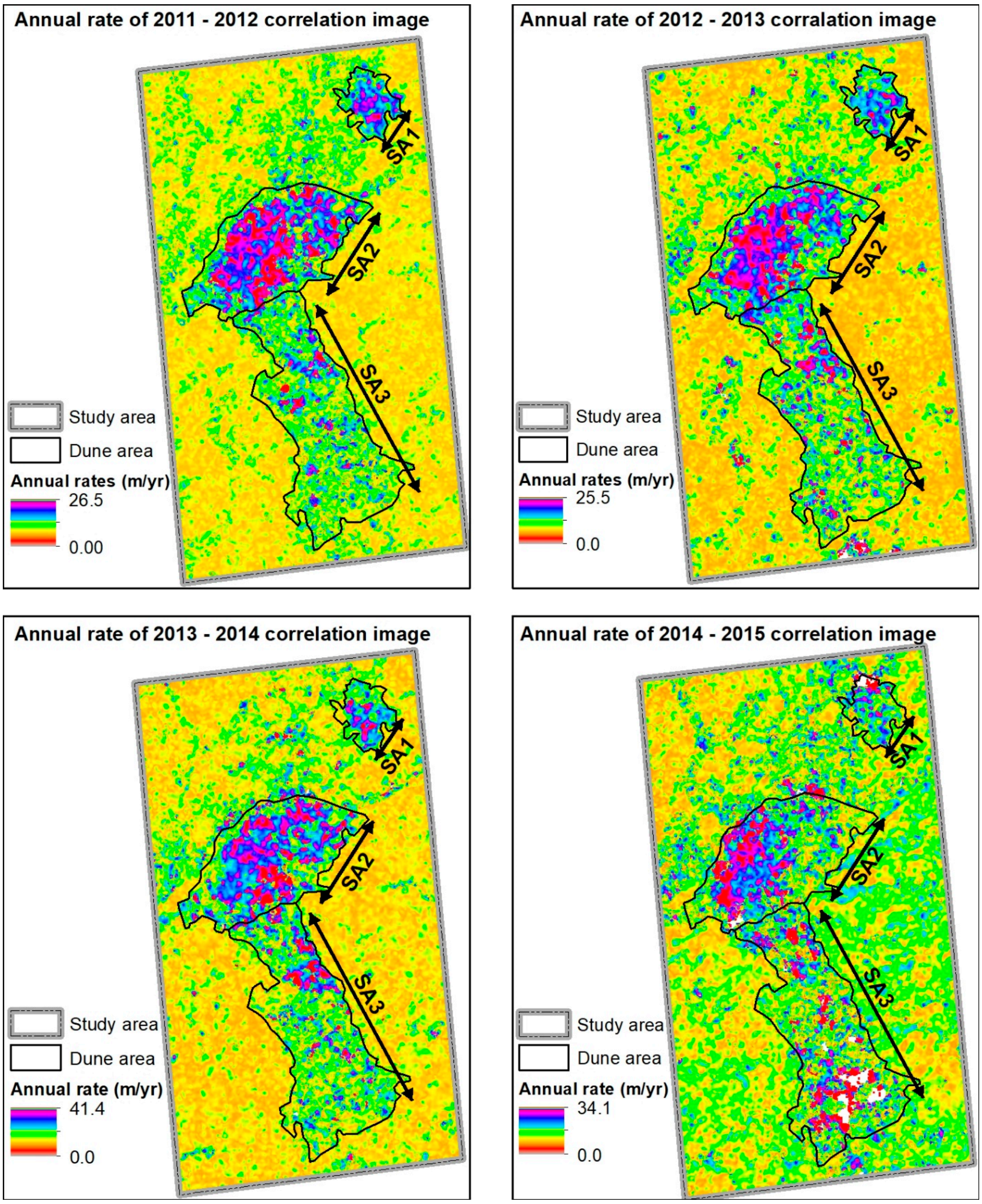

Figure 11. The net annual migration rates through the time period 2011–2015 of the three sand accumulations in the study area.

Table 3 presents the statistics of dune movements within the three sand accumulations. The table rows represent the spatial changes in the magnitude of the annual rates of dune movements within sand accumulations. The table columns represent the temporal changes in the magnitude of the annual rates of dune movements through all sand accumulations.

Table 3. Statistics of the annual migration rates of sand dunes in the three studied sand accumulations.

Correlation Pairs of Annual Rates	Statistics of Annual Rates	Dune Areas			
		SA1	SA2	SA3	Temporal Ranges and Means
2011–2012	Min	0.0	0.0	0.0	0.0
	Max	17.0	26.5	24.3	22.6
	Average	8.1	9.8	5.0	7.6
2012–2013	Min	0.0	0.0	0.0	0.0
	Max	14.8	23.0	24.4	20.7
	Average	6.1	7.2	4.6	6.0
2013–2014	Min	0.0	0.0	0.0	0.0
	Max	22.0	37.8	38.8	32.9
	Average	8.2	10.1	6.2	8.2
2014–2015	Min	0.0	0.0	0.0	0.0
	Max	28.6	30.9	34.1	31.2
	Average	6.5	7.3	6.1	6.6
Accumulative mean (in 4 years)		28.9	34.4	21.6	
Spatial ranges and means	Min	0.0	0.0	0.0	
	Max	20.6	29.6	30.4	
	Means	7.2	8.6	5.5	

Spatial variations in the magnitudes of dune movements are a well-known aspect of sand accumulations worldwide. They vary spatially from one dune area to another, and even among individual dunes in the same dune area [80,81]. This is well demonstrated in the study area where SA2 is characterized by the highest values of the mean annual rates of dune movements (Table 3), ranging from 7.2 to 10.1 m/year, with an average of 8.6 m/year. The second-highest values of the mean annual rates of dune movements were recorded in SA1, ranging from 6.1 to 8.2 m/year, with an average of 7.2 m/year. The lowest magnitudes of the annual rates of dune movements were measured in SA3, ranging from 4.6 to 6.2 m/year, with an average of 5.5 m/year.

Figure 12 clearly expresses the spatio-temporal variations in the mean magnitudes of the annual rates of dune movement in the various sand accumulations. Various implications can be outlined from the analysis of Table 3 and Figure 12. First, the values of the mean annual rates indicate that sand accumulations in the study area are considered active dune areas of moderate magnitude [82]. Second, although the ranges of the mean annual rates between the three dune areas are limited to a few meters annually, the accumulated magnitudes of the mean annual rates over the four-year interval refer to a significant magnitude of dune movements (Table 3). The accumulated means at the end of the four-year interval were 21.6, 28.9, and 34.4 m for SA3, SA1, and SA2, respectively. Third, the magnitudes of the mean annual rates are characterized by the same spatial pattern annually, where SA2 is always the highest, SA1 is intermediate, and SA3 is the lowest (Figure 12). Many factors can be responsible for the spatial pattern of the magnitude of the annual rates. These factors include the spatial locations of sand accumulations and their proximity to sand supply areas. Both SA1 and SA2 are located in the southern reaches of the Wadi Fatmah alluvial plain whereas SA3 is located along Wadi Ash Schumaysi. This exposes SA1 and SA2 of Wadi Fatmah to the predominant northern winds before SA3 of Wadi Ash Shumaysi. Accordingly, SA1 and favorably SA2 have greater opportunity to receive a high sand supply than SA3. In addition, the principal sources of sand supply are more proximal to SA2 and SA1 than to SA3. These sources include the abandoned agricultural areas that are directly located in the northern reaches of these sand accumulations, along with the areas of intensive urban activities and off-road driving. All of these areas represent significant sources of loose sand to be transported by northern winds and deposited where various obstacles are available in the areas of SA1 and SA2. Although SA1 and SA2 have higher magnitudes of dune movements than SA3, SA2 in particular is considered the highest active dune area in the study area. Its spatial extent has expanded remarkably from 15 km^2, as monitored from the Corona image acquired in 1972, to 26 km^2, as mapped from the SPOT 5 image acquired in 2013. The vast spatial expansion of SA2 throughout these few decades strongly implies persistent and potential sand transportation rates [83] that have eventually resulted in a high magnitude of dune movement [1]. Fourth, along with the spatial pattern variations in the magnitude of the annual dune movements, the magnitudes of the mean annual rates show a temporal pattern of dune movements through all dune areas (Figure 12). The temporal variations of the mean annual rates of the three dune areas show consistent patterns, which fluctuate between high and low values through the time interval of the study (Figure 12). The consistency in the fluctuation of temporal magnitudes of dune movements could potentially point to consistent temporal changes in wind intensity on an annual basis. However, the degree of temporal fluctuation in the annual dune migrations of both SA1 and SA2 is higher than that of SA3 (Figure 12), which could be attributed to variations in the local conditions of wind systems [84–86]. Finally, although the degree of temporal fluctuation and mean annual rates of dune movements are generally low for SA3 in the first two sequential years, the last two years have higher magnitudes and almost the same degree of fluctuation in the annual rates of dune movements. The relatively high magnitudes of the annual rates of dune movements in SA3 in the last two sequential years could be linked to the accelerated excavation processes in the mountain blocks located in the northwest corner of Wadi Ash Shumaysi.

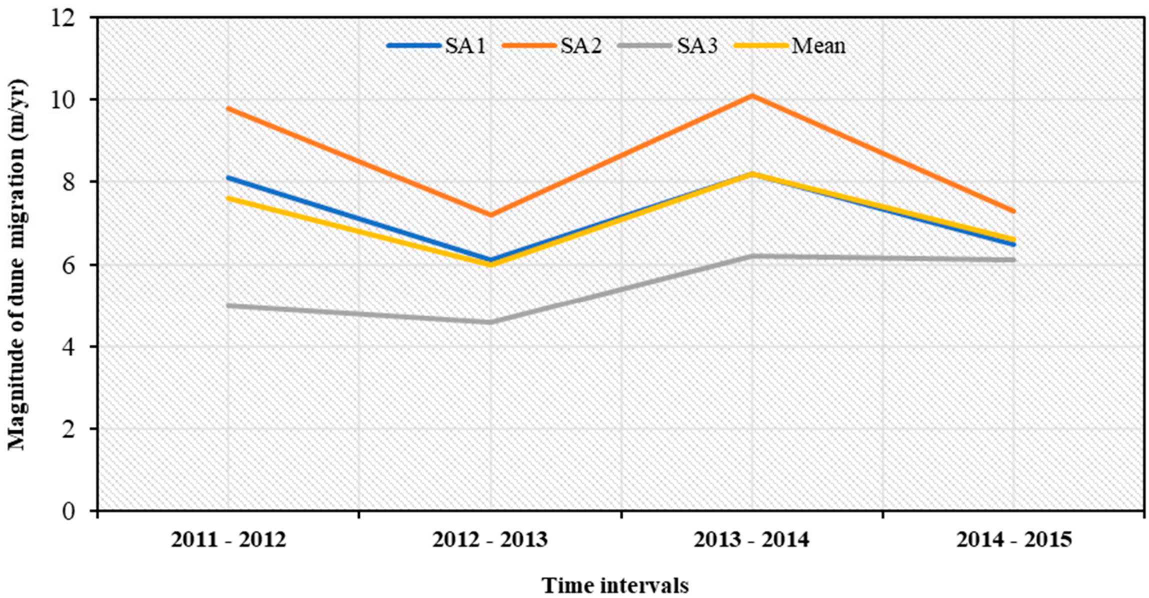

Figure 12. The spatio-temporal variation in the mean annual rates of dune migration of the three sand accumulations in the study area.

6. Conclusions

The previous literature and long archived remote sensing images indicate that the study area in the middle zone of Wadi Fatmah was once a dominant agricultural rural community. There was enough water for agriculture to flourish. Soil moisture ensured widespread bushes in the southern bank of the trunk valley of Wadi Fatmah drainage basin. Sand accumulations were limited to areas adjacent to the western mountain block and slowly interfered with bushes westward. Earth observation satellites allowed us to retrieve the spatial features of the landscapes in the study area, and to analyze their spatial relationships. The unmanaged water discharge and water harvesting strategy adopted in the study area along with unplanned agricultural practices represented the main driving forces that resulted in extensive changes in the landscape of the study area. Over the last five decades, surface runoff from the upstream basins of Wadi Fatmah has been controlled by Wadi Fatmah Dam, depriving the alluvial deposits in the middle zone where the study area is located from intermittent water recharge. Extensive pumping of the shallow alluvial aquifers in the area to meet the water requirements of the adjacent big cities has maximized water deficiency as well. Under such circumstances, along with the severe arid conditions, agricultural areas have been abandoned, allowing intensive wind erosion of the soil to occur. These processes have increased sand supply to sand accumulations in the study area. The conversion of the landscape from simple rural agricultural land into a more urbanized landscape has allowed more off-road driving and excavation activities to occur over the alluvial plains and bajada surfaces as well as at the top of the many mountain blocks adjacent to the alluvial plains. These activities have created loose sands capable of being transported by the wind into sand accumulations in the study area, which has resulted in e the spatial extents of these accumulations being enlarged and enabled significant rates of dune migration. These processes indicate that unmanaged and unplanned anthropogenic interferences have caused the environmental system in the study area to be transformed from one state to another. The massive retreat of vegetation cover associated with extensive expansion of sand accumulations that characterize the recent state of the environmental system indicate that the study area may undergo desertification processes. The results of this current research are useful in supporting decision-making processes that may be interested in combating desertification processes and conserving the natural resources in the study area.

Author Contributions: Conceptualization, E.H.; methodology, E.H., O.A., A.A. and A.J.N.; software, E.H. and A.J.N.; validation, E.H., O.A., A.A. and A.J.N.; formal analysis, E.H.; investigation, E.H.; resources, E.H., O.A., A.A., A.J.N., K.A.-G., M.A.-M. and A.F.; data curation, E.H., A.J.N. and K.A.-G.; writing—original draft preparation, E.H.; writing—review and editing, E.H.; visualization, E.H.

Funding: This research received no external funding.

Acknowledgments: Authors would like to thank the King Abdulaziz City for Science and Technology (KACST) for providing SPOT-5 Data.

Conflicts of Interest: The authors declare no conflict of interest.

References

1. Lancaster, N. Dune Morphology and Dynamics. In *Geomorphology of Desert Environments*; Parsons, A.J., Abrahams, A.D., Eds.; Springer: Dordrecht, The Netherlands, 2009; pp. 557–595. [CrossRef]
2. Nordstrom, K.F.; Psuty, N.; Carter, B. *Coastal Dunes: Form and Process*; Wiley: New York, NY, USA, 1990.
3. Wilson, I.G. Ergs. *Sediment. Geol.* **1973**, *10*, 77–106. [CrossRef]
4. Fryberger, S.G.; Ahlbrandt, T.S.; Andrews, S. Origin, sedimentary features, and significance of low-angle eolian "sand sheet" deposits, Great Sand Dunes National Monument and vicinity, Colorado. *J. Sediment. Res.* **1979**, *49*, 733–746. [CrossRef]
5. Whitney, J.W. *Erosional History and Surficial Geology of Western Saudi Arabia. Technical Report USGS-TR-04-1*; Ministry of Petroleum and Mineral Resources: Jeddah, Saudi Arabia, 1983.
6. Al-Harthi, A. Geohazard assessment of sand dunes between Jeddah and Al-Lith, western Saudi Arabia. *Environ. Geol.* **2002**, *42*, 360–369. [CrossRef]
7. White, B.R.; Tsoar, H. Slope effect on saltation over a climbing sand dune. *Geomorphology* **1998**, *22*, 159–180. [CrossRef]
8. Bauer, B.O.; Davidson-Arnott, R.G.D. A general framework for modeling sediment supply to coastal dunes including wind angle, beach geometry, and fetch effects. *Geomorphology* **2003**, *49*, 89–108. [CrossRef]
9. Iversen, J.D.; Rasmussen, K.R. The effect of wind speed and bed slope on sand transport. *Sedimentology* **1999**, *46*, 723–731. [CrossRef]

10. Qian, G.; Dong, Z.; Luo, W.; Lu, J. Mean airflow patterns upwind of topographic obstacles and their implications for the formation of echo dunes: A wind tunnel simulation of the effects of windward slope. *J. Geophys. Res. Earth Surf.* **2011**, *116*. [CrossRef]
11. Livingstone, I.; Warren, A. *Aeolian Geomorphology: An Introduction*; Longman: London, UK, 1996.
12. Ren, J.; Zhang, S.; Meigs, A.J.; Yeats, R.S.; Ding, R.; Shen, X. Tectonic controls for transverse drainage and timing of the Xin-Ding paleolake breach in the upper reach of the Hutuo River, north China. *Geomorphology* **2014**, *206*, 452–467. [CrossRef]
13. Lorenz, R.D.; Zimbelman, J.R. *Dune Worlds: How Windblown Sand Shapes Planetary Landscapes*; Springer Science & Business Media: New York, NY, USA, 2014.
14. Muhs, D.R. Evaluation of simple geochemical indicators of aeolian sand provenance: Late Quaternary dune fields of North America revisited. *Quat. Sci. Rev.* **2017**, *171*, 260–296. [CrossRef]
15. Al-Naji, A.J.; Al-Shammery, T.A. Mineralogical study of Sand Dunes Fields in Najaf Governorate, Southern Iraq. *Iraqi J. Sci.* **2019**, *60*, 239–254.
16. Lancaster, N.; Baas, A. Influence of vegetation cover on sand transport by wind: Field studies at Owens Lake, California. *Earth Surf. Process. Landf.* **1998**, *23*, 69–82. [CrossRef]
17. Tsoar, H. Sand dunes mobility and stability in relation to climate. *Phys. A Stat. Mech. Appl.* **2005**, *357*, 50–56. [CrossRef]
18. Forman, S.L.; Oglesby, R.; Webb, R.S. Temporal and spatial patterns of Holocene dune activity on the Great Plains of North America: Megadroughts and climate links. *Glob. Planet. Chang.* **2001**, *29*, 1–29. [CrossRef]
19. Amir, R.; Kinast, S.; Tsoar, H.; Yizhaq, H.; Zaady, E.; Ashkenazy, Y. The effect of wind and precipitation on vegetation and biogenic crust covers in the Sde-Hallamish sand dunes. *J. Geophys. Res. Earth Surf.* **2014**, *119*, 437–450. [CrossRef]
20. Wu, J.; Loucks, O.L. From Balance of Nature to Hierarchical Patch Dynamics: A Paradigm Shift in Ecology. *Q. Rev. Biol.* **1995**, *70*, 439–466. [CrossRef]
21. Seifan, M. Long-term effects of anthropogenic activities on semi-arid sand dunes. *J. Arid Environ.* **2009**, *73*, 332–337. [CrossRef]
22. Tsoar, H. The ecological background, deterioration and reclamation of desert dune sand. *Agric. Ecosyst. Environ.* **1990**, *33*, 147–170. [CrossRef]
23. Schlesinger, W.H.; Reynolds, J.F.; Cunningham, G.L.; Huenneke, L.F.; Jarrell, W.M.; Virginia, R.A.; Whitford, W.G. Biological feedbacks in global desertification. *Science* **1990**, *247*, 1043–1048. [CrossRef]
24. Briske, D.D.; Fuhlendorf, S.D.; Smeins, F.E. Vegetation dynamics on rangelands: A critique of the current paradigms. *J. Appl. Ecol.* **2003**, *40*, 601–614. [CrossRef]
25. Marín, L.; Forman, S.L.; Valdez, A.; Bunch, F. Twentieth century dune migration at the Great Sand Dunes National Park and Preserve, Colorado, relation to drought variability. *Geomorphology* **2005**, *70*, 163–183. [CrossRef]
26. Danielsen, R.; Castilho, A.M.; Dinis, P.A.; Almeida, A.C.; Callapez, P.M. Holocene interplay between a dune field and coastal lakes in the Quiaios—Tocha region, central littoral Portugal. *Holocene* **2012**, *22*, 383–395. [CrossRef]
27. Al-Hurban, A.E. Effects of recent anthropogenic activities on the surface deposits of Kuwait. *Arab. J. Geosci.* **2014**, *7*, 665–691. [CrossRef]
28. Cabrera-Vega, L.L.; Cruz-Avero, N.; Hernández-Calvento, L.; Hernández-Cordero, A.I.; Fernández-Cabrera, E. Morphological changes in dunes as an indicator of anthropogenic interferences in arid dune fields. *J. Coast. Res.* **2013**, *65*, 1271–1276. [CrossRef]
29. Roskin, J.; Sivan, D.; Shtienberg, G.; Roskin, E.; Porat, N.; Bookman, R. Natural and human controls of the Holocene evolution of the beach, aeolian sand and dunes of Caesarea (Israel). *Aeolian Res.* **2015**, *19*, 65–85. [CrossRef]
30. McKee, E.D. Introduction to a study of global sand seas. In *A Study of Global Sand Seas*; U.S. Geological Survey Professional Paper: Reston, VA, USA, 1979; Volume 1052, pp. 1–19.
31. Breed, C.S.; Fryberger, S.G.; Andrews, S.; McCauley, C.; Lennartz, F.; Gebel, D.; Horstman, K. Regional studies of sand seas using Landsat (ERTS) imagery. In *A Study of Global Sand Seas*; U.S. Geological Survey Professional Paper: Reston, VA, USA, 1979; Volume 1052, pp. 305–397.
32. Ewing, R.C.; Kocurek, G.; Lake, L.W. Pattern analysis of dune-field parameters. *Earth Surf. Process. Landf.* **2006**, *31*, 1176–1191. [CrossRef]

33. Ewing, R.C.; Kocurek, G. Aeolian dune interactions and dune-field pattern formation: White Sands Dune Field, New Mexico. *Sedimentology* **2010**, *57*, 1199–1219. [CrossRef]
34. Ewing, R.C.; Kocurek, G. Aeolian dune-field pattern boundary conditions. *Geomorphology* **2010**, *114*, 175–187. [CrossRef]
35. Hugenholtz, C.H.; Barchyn, T.E. Spatial analysis of sand dunes with a new global topographic dataset: New approaches and opportunities. *Earth Surf. Process. Landf.* **2010**, *35*, 986–992. [CrossRef]
36. Hugenholtz, C.H.; Levin, N.; Barchyn, T.E.; Baddock, M.C. Remote sensing and spatial analysis of aeolian sand dunes: A review and outlook. *Earth Sci. Rev.* **2012**, *111*, 319–334. [CrossRef]
37. Blumberg, D.G. Remote Sensing of Desert Dune Forms by Polarimetric Synthetic Aperture Radar (SAR). *Remote Sens. Environ.* **1998**, *65*, 204–216. [CrossRef]
38. Levin, N.; Ben-Dor, E.; Karnieli, A. Topographic information of sand dunes as extracted from shading effects using Landsat images. *Remote Sens. Environ.* **2004**, *90*, 190–209. [CrossRef]
39. Ojeda, J.; Vallejo, I.; Malvarez, G.C. Morphometric evolution of the active dunes system of the Doñana National Park, Southern Spain (1977–1999). *J. Coast. Res.* **2005**, *49*, 40–45.
40. Kocurek, G.A. Desert aeolian systems. In *Sedimentary Environments: Processes, Facies and Stratigraphy*, 3rd ed.; Reading, H.G., Ed.; Blackwell: Oxford, UK, 1996.
41. Hugenholtz, C.H.; Wolfe, S.A. Biogeomorphic model of dunefield activation and stabilization on the northern Great Plains. *Geomorphology* **2005**, *70*, 53–70. [CrossRef]
42. Finkel, H.J. The Barchans of Southern Peru. *J. Geol.* **1959**, *67*, 614–647. [CrossRef]
43. Merk, G.P. Dune Form and Structure at Great Sand Dunes National Monument. Doctoral Dissertation, University of Colorado, Boulder, CO, USA, 1962.
44. Long, J.T.; Sharp, R.P. Barchan-dune movement in imperial valley, California. *Geol. Soc. Am. Bull.* **1964**, *75*, 149–156. [CrossRef]
45. Calkin, P.E.; Rutford, R.H. The sand dunes of Victoria Valley, Antarctica. *Geogr. Rev.* **1974**, *64*, 189–216. [CrossRef]
46. Wiegand, J.P. Dune Morphology and Sedimentology at Great Sand Dunes National Monument. Doctoral Dissertation, Colorado State University, Fort Collins, CO, USA, 1977.
47. Maxwell, T.A.; Haynes, C.V. Sand sheet dynamics and Quaternary landscape evolution of the Selima Sand Sheet, southern Egypt. *Quat. Sci. Rev.* **2001**, *20*, 1623–1647. [CrossRef]
48. Aql, M.T. Movement of sands east Suez Canal and its impact on human activities: A study in applied geomorphology. *Al Ensaniat* **2002**, *19*, 1–75. (In Arabic)
49. Mitasova, H.; Overton, M.; Harmon, R.S. Geospatial analysis of a coastal sand dune field evolution: Jockey's Ridge, North Carolina. *Geomorphology* **2005**, *72*, 204–221. [CrossRef]
50. Bourke, M.C.; Ewing, R.C.; Finnegan, D.; McGowan, H.A. Sand dune movement in the Victoria Valley, Antarctica. *Geomorphology* **2009**, *109*, 148–160. [CrossRef]
51. Tsoar, H. *The Dynamics of Longitudinal Dunes: Final Technical Report*; U.S. Army; European Research Office: London, UK, 1978; p. 171.
52. Tsoar, H.; Blumberg, D.G.; Stoler, Y. Elongation and migration of sand dunes. *Geomorphology* **2004**, *57*, 293–302. [CrossRef]
53. Liu, J.G.; Capes, R.; Haynes, M.; Moore, J.M. ERS SAR multi-temporal coherence image as a tool for sand desert study (sand movement, sand encroachment and erosion). In Proceedings of the 12th International Conference and Workshop on Applied Geologic Remote Sensing, Denver, CO, USA, 17–19 November 1997; pp. I-478–I-485.
54. Leprince, S.; Barbot, S.; Ayoub, F.; Avouac, J. Automatic and precise orthorectification, coregistration, and subpixel correlation of satellite images, application to ground deformation measurements. *IEEE Trans. Geosci. Remote Sens.* **2007**, *45*, 1529–1558. [CrossRef]
55. Hermas, E.A. Monitoring the spatial occurrences and migration rates of sand dunes around Makkah city using remote sensing technology. *Remote Sens. GIS* **2015**, *3*, 14–24.
56. Vermeesch, P.; Drake, N. Remotely sensed dune celerity and sand flux measurements of the world's fastest barchans (Bodélé, Chad). *Geophys. Res. Lett.* **2008**, *35*. [CrossRef]
57. Necsoiu, M.; Leprince, S.; Hooper, D.M.; Dinwiddie, C.L.; McGinnis, R.N.; Walter, G.R. Monitoring migration rates of an active subarctic dune field using optical imagery. *Remote Sens. Environ.* **2009**, *113*, 2441–2447. [CrossRef]

58. Hermas, E.A.; Leprince, S.; El-Magd, I.A. Retrieving sand dune movements using sub-pixel correlation of multi-temporal optical remote sensing imagery, northwest Sinai Peninsula, Egypt. *Remote Sens. Environ.* **2012**, *121*, 51–60. [CrossRef]
59. Al-Ghamdi, K.A.; Hermas, E.A. Assessment of dune migration hazards against landuse northwest Al-lith City, Saudi Arabia, using multi-temporal satellite imagery. *Arab. J. Geosci.* **2015**, *8*, 11007–11018. [CrossRef]
60. Al-Mutiry, M.; Hermas, E.A.; Al-Ghamdi, K.A.; Al-Awaji, H. Estimation of dune migration rates north Riyadh City, KSA, using SPOT 4 panchromatic images. *J. Afr. Earth Sci.* **2016**, *124*, 258–269. [CrossRef]
61. Hamandawana, H.; Eckardt, F.; Ringrose, S. The use of step-wise density slicing in classifying high-resolution panchromatic photographs. *Int. J. Remote Sens.* **2006**, *27*, 4923–4942. [CrossRef]
62. Herrmann, S.M.; Wickhorst, A.J.; Marsh, S.E. Estimation of Tree Cover in an Agricultural Parkland of Senegal Using Rule-Based Regression Tree Modeling. *Remote Sens.* **2013**, *5*, 4900–4918. [CrossRef]
63. Ayoub, F.; Leprince, S.; Keene, L. *User's Guide to COSI-CORR Co-Registration of Optically Sensed Images and Correlation*; California Institude of Tecnology: Pasadena, CA, USA, 2009; p. 38.
64. Buades, A.; Coll, B.; Morel, J. Nonlocal Image and Movie Denoising. *Int. J. Comput. Vis.* **2008**, *76*, 123–139. [CrossRef]
65. Simons, M. *The Changing World Deserts: The Problem of Water in Arid Lands*; Oxford University Press: London, UK, 1967.
66. Al-Harbi, N.M. Geomorphic Units and Their Relationships with Land Use and Land Cover in the Drainage Basin of Wadi. Ph.D. Thesis, Umm Al-Qura University, Makkah, Saudi Arabia, 2017. (In Arabic).
67. Sadhan, A.S. Water Plan for Wadi Fatimah Basin, Saudi Arabia. Doctoral Dissertation, University of Wyoming, Laramie, WY, USA, 1980.
68. Alrhiliy, A.A. Climate Characteristics in Makkah Administrative Area. Ph.D. Thesis, Umm Al-Qura University, Makkah, Saudi Arabia, 2010. (In Arabic).
69. Al-Mealem, A.A. Geomorphology of Hassan Basin in Yemen. Ph.D. Thesis, Baghdad University, Baghdad, Iraq, 2004. (In Arabic).
70. Hamimi, Z.; Matsah, M.; El-Shafei, M.; El-Fakharani, A.; Shujoon, A.; Al-Gabali, M. Wadi Fatima thin-skinned foreland FAT belt: A post amalgamation marine basin in the Arabian Shield. *Open J. Geol.* **2012**, *2*, 271. [CrossRef]
71. Pye, K.; Tsoar, H. Aeolian Bed Forms. In *Aeolian Sand and Sand Dunes*; Springer: Berlin/Heidelberg, Germany, 2009; pp. 175–253. [CrossRef]
72. AlJumaie, Z.M. Possibilities of Agricultural Development in Wadi Fatmah of Makkah Al-Mukarramah: An Applied Study on Agricultural Capabilities. Master's Thesis, Umm Al-Qura University, Makkah, Saudi Arabia, 1990. (In Arabic).
73. El-Barodi, M.S. Water Balance Estimates of Wadi Fatmah Basin. *J. Kuwait Geogr. Soc.* **1986**, *88*, 5–60. (In Arabic)
74. Schlesinger, W.H.; Fonteyn, P.J.; Reiners, W.A. Effects of Overland Flow on Plant Water Relations, Erosion, and Soil Water Percolation on a Mojave Desert Landscape. *Soil Sci. Soc. Am. J.* **1989**, *53*, 1567–1572. [CrossRef]
75. Muhs, D.R.; Been, J.; Mahan, S.A.; Burdett, J.; Skipp, G.; Rowland, Z.M.; Stafford, T.W., Jr. Holocene eolian activity in the Minot dune field, North Dakota. *Can. J. Earth Sci.* **1997**, *34*, 1442–1459. [CrossRef]
76. Huenneke, L.F.; Anderson, J.P.; Remmenga, M.; Schlesinger, W.H. Desertification alters patterns of aboveground net primary production in Chihuahuan ecosystems. *Glob. Chang. Biol.* **2002**, *8*, 247–264. [CrossRef]
77. Meir, A.; Tsoar, H. International borders and range ecology: The case of Bedouin transborder grazing. *Hum. Ecol.* **1996**, *24*, 39–64. [CrossRef]
78. Tsoar, H. Critical Environments: Sand Dunes and Climate Change. In *Treatise on Geomorphology, Aeolian Geomorphology*; Shroder, J.F., Lancaster, N., Sherman, D.J., Baas, A.C.W., Eds.; Academic Press: San Diego, CA, USA, 2013; Volume 11, pp. 414–427.
79. Necsoiu, M.; Hooper, D.; Roseberry, J. Physical properties of volcanic material (tephra) using visible near-infrared spectroscopy. In Proceedings of the AGU Fall Meeting Abstracts, San Francisco, CA, USA, 9–13 December 2019.
80. Ali, A. The Geomorphology of Sand Dunes of South and Southeast Qattara Depression. Ph.D. Thesis, Ain Shams University, Cairo, Egypt, 1993.
81. Tsoar, H. Dynamic processes acting on a longitudinal (seif) sand dune. *Sedimentology* **1983**, *30*, 567–578. [CrossRef]

82. Misak, R.F.; El Ghazawy, M.M. Desertification Processes in the Sinai Peninsula, Egypt. In Proceedings of the International Meeting on Environmental Disasters and Desertification, Palermo, Italy, 16 June 1989.
83. Scheidt, S.P.; Lancaster, N. The application of COSI-Corr to determine dune system dynamics in the southern Namib Desert using ASTER data. *Earth Surf. Process. Landf.* **2013**, *38*, 1004–1019. [CrossRef]
84. Tsoar, H. Desert dunes morphology and dynamics, El Arish, northern Sinai. *Z. Geomorphol.* **1974**, *20*, 41–61.
85. Assal, E.M. Sedimentological Studies on the Quaternary Sand Dunes and Sabkhas. Master's Thesis, Damiatta Faculty of Science, University of Mansura, Northern Sinai, Egypt, 1999; p. 268.
86. Embabi, N.S. *Landscapes and Landforms of Egypt*; Springer: Cham, Switzerland, 2018.